Design and Validation of Sensorized Tools for Deformable Object Manipulation in Meat Cutting and Doll Demoulding

Saltanat Seitzhan[1][a], Dionisio Cartagena González[2][b], Alexis Babut[3][c], Daniel Sánchez-Martínez[2][d], Juan Antonio Micó[2], Chedli Bouzgarrou[3][e] and Juan Antonio Corrales Ramón[1][f]

[1]*Universidade de Santiago de Compostela, Santiago de Compostela, Spain*

[2]*AIJU Technological Institute for Children's Products and Leisure, Alicante, Spain*

[3]*Université Clermont Auvergne, Clermont Auvergne INP, CNRS, Institut Pascal F-63000 Clermont-Ferrand, France*

Keywords: Sensorized Tools, Soft Robotics, Demoulding, Meat Cutting, Force Sensing, Learning by Demonstration, Collaborative Robots, Automation.

Abstract: While robotic arms are extensively deployed in mass production environments, their application in tasks involving deformable object manipulation remains limited due to the complex dynamics of soft materials. Addressing this challenge requires task-specific end-effector tools capable of replicating manual operations with precision and adaptability. Standard human tools are often incompatible with robotic systems, especially in domains such as meat processing and doll manufacturing. This study presents the design and experimental validation of sensor-integrated end-effectors tailored for deformable object handling: a knife tool for robotic-assisted meat cutting and a plier tool for analyzing the demoulding process in doll production. Both tools incorporate multimodal sensing, including force/torque sensors and inertial measurement units, and are synchronized via ROS to capture manipulation data under realistic conditions. While full cobotic manipulation and Learning from Demonstration (LfD) are reserved for future work, the results demonstrate the feasibility of embedding sensing into manual and robotic tools to support future automation in soft material handling.

1 INTRODUCTION

The manipulation of deformable objects poses persistent challenges in robotics due to the unpredictable and nonlinear behavior of soft materials. While automation has made significant strides in rigid object handling, tasks involving soft components such as cutting, gripping, or assembly remain largely dependent on human expertise. This limitation is particularly evident in industrial domains like meat processing and toy manufacturing, where the complexity of soft object interactions continues to hinder full automation.

In the meat industry, for example, the irregularity of meat pieces has led to the adoption of robotic assistance rather than full automation for cutting tasks. Despite advances in sensing and modeling, the variability in tissue structure, fat distribution, and carcass geometry makes it difficult to generalize cutting strategies across specimens. Robotic systems have been deployed for tasks such as primal cutting and trimming, often relying on preoperative scanning or vision-based guidance (Aly et al., 2023; Mason et al., 2022). However, full automation remains elusive, and collaborative approaches, such as human-in-the-loop systems or sensorized tools, are increasingly explored to capture expert manipulation strategies (Maithani et al., 2021).

Similarly, in doll production, processes like demoulding and assembly of vinyl parts are still performed manually due to the complexity of soft object interactions. Recent efforts have explored automation in these domains, with varying degrees of success. In toy manufacturing, collaborative robotic

[a] https://orcid.org/0009-0002-0620-9617
[b] https://orcid.org/0009-0003-3060-7815
[c] https://orcid.org/0009-0005-2749-1422
[d] https://orcid.org/0009-0008-2279-3503
[e] https://orcid.org/0000-0003-2394-1770
[f] https://orcid.org/0000-0002-9373-7954

Seitzhan, S., González, D. C., Babut, A., Sánchez-Martínez, D., Micó, J. A., Bouzgarrou, C. and Corrales Ramón, J. A.
Design and Validation of Sensorized Tools for Deformable Object Manipulation in Meat Cutting and Doll Demoulding.
DOI: 10.5220/0013967900003982

In *Proceedings of the 22nd International Conference on Informatics in Control, Automation and Robotics (ICINCO 2025) - Volume 2*, pages 552-565
ISBN: 978-989-758-770-2; ISSN: 2184-2809

systems have been deployed to automate demoulding tasks using vision-guided manipulation and custom grippers with embedded force control (Sánchez-Martínez et al., 2023). In parallel, research in robotic learning has demonstrated the potential of sensorized tools to capture human manipulation strategies, particularly within Learning from Demonstration (LfD) frameworks (Song et al., 2022; Zakaria et al., 2022). These tools enable the recording of multimodal data including force, motion, and orientation under realistic working conditions, facilitating the transfer of human skills to robotic platforms.

This paper builds upon these developments and proposes two fully embedded sensorized handheld tools. Firstly, a sensor-implemented knife end-effector series with different variations of sensor placement along with tactile-sensitive handle. Secondly, a sensor-implemented plier tool designed to capture human demonstrations during soft object manipulation. The remainder of this paper is organized as follows: Section 2 reviews related work; Section 3 describes the tool design and instrumentation; Section 4 presents experimental validation; and Section 6 concludes the paper. The key contributions of this work are as follows:

- Design of sensorized end-effectors tailored for deformable object manipulation in industrial contexts, specifically meat cutting and doll demoulding.
- Integration of multimodal sensing (force, orientation, tactile pressure) into ergonomic handheld tools to capture human demonstrations without disrupting natural behavior.

2 BACKGROUND

2.1 Meat Cutting

The automation of meat processing presents a solution to address persistent challenges in labor-intensive, hazardous, and hygiene-sensitive environments. The red meat industry, particularly in cutting and deboning operations, is characterized by repetitive tasks, exposure to cold temperatures, and high injury rates, making it a prime candidate for robotic intervention (Aly et al., 2023).

Earlier work by Choi et al. (Choi et al., 2013) highlighted the potential of industrial robots to alleviate ergonomic strain and improve consistency in meat processing. Their study emphasized the importance of integrating force control and vision systems to navigate the variability inherent in carcass morphology. However, the complexity of handling deformable biological materials such as muscle, fat, and connective tissue has limited the adoption of robotic systems beyond simple, rigid tasks.

Recent advances have focused on enhancing robotic perception and adaptability. Aly et al. (Aly et al., 2023) provided a comprehensive review of sensing technologies in red meat processing, identifying X-ray, ultrasonic, optical probes, and tactile sensing as key enablers for trajectory planning and adaptive control. Their analysis underscored the limitations of preoperative scanning alone and advocated for hybrid systems combining real-time feedback with anatomical modeling.

In parallel, the RoBUTCHER project introduced the concept of the Meat Factory Cell (MFC), a modular robotic platform designed for hot boning and autonomous disassembly of pig carcasses (de Medeiros Esper et al., 2021). This system leverages RGB-D vision, computed tomography, and machine learning to plan and execute cuts, while addressing hygiene and scalability concerns. Building on this, Mason et al. (Mason et al., 2022) developed a smart knife equipped with electromagnetic sensing, capable of detecting contact and cutting depth with high precision. This tool demonstrated the feasibility of integrating sensorized end-effectors into robotic workflows, enabling real-time feedback and adaptive control.

Complementary studies have investigated robotic manipulation of deformable objects using mass-spring models, structured light, and force feedback (Long et al., 2014a; Long et al., 2014b; Nabil et al., 2015). These approaches aim to simulate tissue behavior and inform control strategies, though challenges remain in achieving real-time responsiveness and generalization across carcass types.

Our previous work on Exoscarne (Maithani et al., 2021) explored human-robot collaboration in meat cutting, proposing assistive strategies that combine physical human-robot interaction with trajectory guidance. By leveraging the operator's expertise and tactile perception, Exoscarne reduced cutting effort and improved safety, laying the groundwork for semi-autonomous systems in complex tasks. The current study builds upon this progress by introducing reactive, friction-reducing features in the robotic cutting tool.

2.2 Doll Industry Automation

The automation of manual tasks involving complex interaction with deformable objects remains a significant challenge in industrial robotics. Captur-

ing and transferring a human operator's manipulation strategy to a collaborative robot requires sensorized tools capable of recording both trajectories and applied forces. Several studies have addressed this through Learning from Demonstration (LfD), often relying on external sensors like motion capture or wrist-mounted force/torque sensors, which limit real-world applicability due to occlusion and calibration issues. The SoftManBot project demonstrated the feasibility of using task-specific sensorized tools for soft object handling in toy manufacturing (Sánchez-Martínez et al., 2023). However, early prototypes lacked embedded force sensing. Recent work has advanced this by integrating tactile arrays (Song et al., 2022) and inline force sensing (Zakaria et al., 2022), enabling dynamic grasp evaluation and DRL-based control of soft linear objects. Building on these insights, we propose a fully embedded, multimodal sensorized tool for capturing human demonstrations under real working conditions.

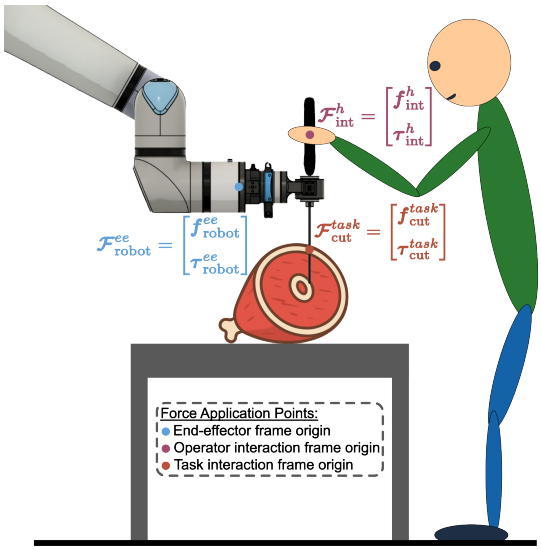

Figure 1: Forces applied on the tool during a meat-cutting task with a robot.

3 DESIGN OF THE SENSORIZED TOOLS

3.1 Knife End-Effector for Meat Cutting

This section presents the development of the instrumented tool mounted on the robot's tool flange (UR30), with a focus on its mechanical integration and force/torque (F/T) sensing capabilities. The tool is designed to accurately perceive contact between the human operator and the manipulated object during task execution.

Another key design consideration was to closely replicate the tools commonly used in the meat-cutting industry. Thus, the distance between the knife handle and the blade was minimised to prevent the operator from experiencing an unnatural sensation caused by an excessively long gap relative to the handle.

3.1.1 Sensor Integration at the Robot Tool Flange

To enable reliable force sensing, an F/T sensor is mounted on the tool flange of the UR30 collaborative robot. Two main sensor models have been used depending on the setup: either the BOTA Systems SensONE T15 or the BOTA Systems SensONE T80. The choice of sensor depends on the specific requirements and mechanical constraints of each experimental configuration.

(a) SensONE T15

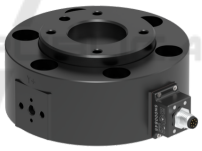

(b) SensONE T80

Figure 2: BOTA Systems SensONE sensors.

The SensONE T80 sensor is directly compatible with the UR30 flange, while the T15 requires a custom mechanical adapter. This adapter, manufactured by FDM (Fused Deposition Modeling) 3D printing in PA-CF (Nylon reinforced with carbon fibre), ensures proper sensor integration.

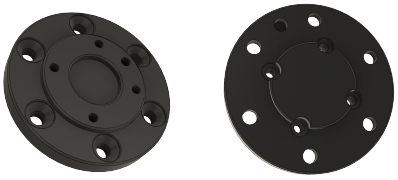

(a) Sensor side (b) Robot side

Figure 3: PA-CF adapter for the SensONE T15 sensor.

Since the tool is subjected to forces from both the operator and the cutting interaction, a single sensor

cannot distinguish between them. To address this, a second sensor (BOTA Systems Rokubi) is added to isolate and measure these forces independently. This also opens the possibility to prototype a design incorporating two additional Rokubi sensors, adding redundancy and enabling direct measurement of cutting and operator-applied forces. Two main configurations were developed for the knife prototype at the end-effector, each positioned after the primary F/T sensor.

3.1.2 Single-Sensor Configuration for Force Isolation

A single Rokubi sensor is integrated to directly measure either the forces applied by the operator or those resulting from interaction with the task. The SensONE sensor continues to measure the overall force data and the main sensor is used to estimate the cutting forces. This approach requires an accurate evaluation of the tool's weight and centre of mass to ensure correct force estimation.

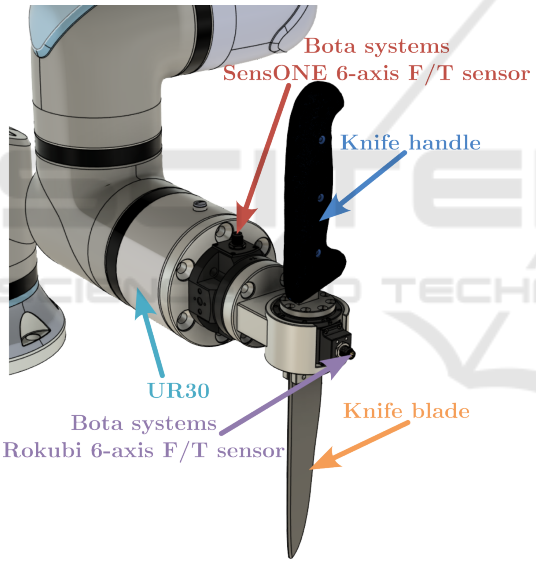

Figure 4: Knife prototype with one additional F/T sensor.

As the forces involved in the cutting task do not exceed a maximum of 200 N, as confirmed by a previous force evaluation shown in Figure 5, three prototypes with identical dimensions and geometry were developed. One prototype was machined from aluminium 5083, another was manufactured using FDM 3D printing with polyamide PA12, and the third was produced using FDM 3D printing with PA-CF, a polyamide reinforced with short carbon fibres. These material variants enable a comparative assessment of stiffness, durability, and overall mechanical performance during meat-cutting operations.

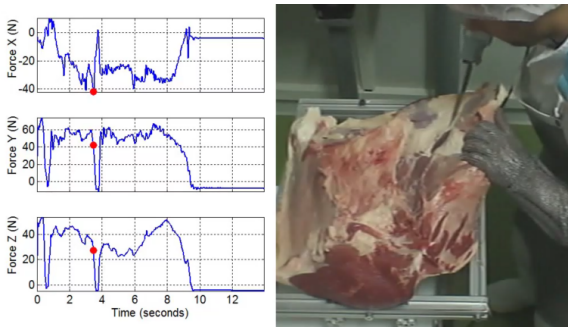

Figure 5: Forces applied during a manual anatomical meat-cutting task.

Metallic Design

In this version, a Rokubi sensor is placed between the main SensONE sensor and the knife. The mounting interface, composed of two machined aluminum parts (or alternatively polyamide PA12 components), is designed symmetrically to allow the entire assembly to be mounted in two orientations. This reversible configuration enables the measurement of either blade-applied forces or handle-applied forces, depending on which component is positioned on the sensor side.

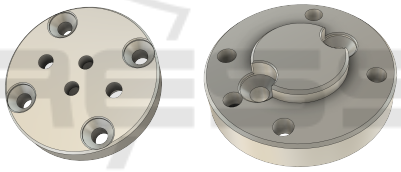

(a) Top view (b) Bottom view

Figure 6: First part of the adapter.

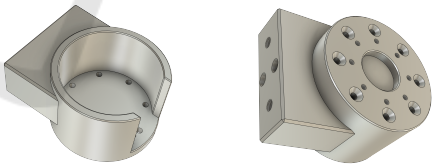

(a) Top view (b) Bottom view

Figure 7: Second part of the adapter.

Both parts include holes for cylindrical alignment dowels to ensure precise positioning between components. Once aligned, the assembly is secured using screws inserted into threaded holes in the metallic parts.

This design allows the sensor to be almost entirely enclosed by the adapter walls, providing mechanical protection and reducing the risk of unintended contact. This minimises the likelihood of measurement disturbances or potential sensor damage during operation.

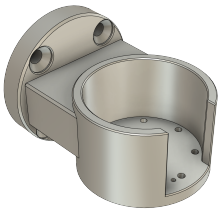

Figure 8: Fully assembled metallic adapter.

PA-CF Design

A functionally equivalent version was produced using PA-CF (polyamide reinforced with short carbon fibers) to benefit from its favorable strength-to-weight ratio and rigidity. This lighter design helps reduce the static load on the robot, thereby maximizing the available force capacity for the task (the UR30 robot has a payload limit of 30 kg).

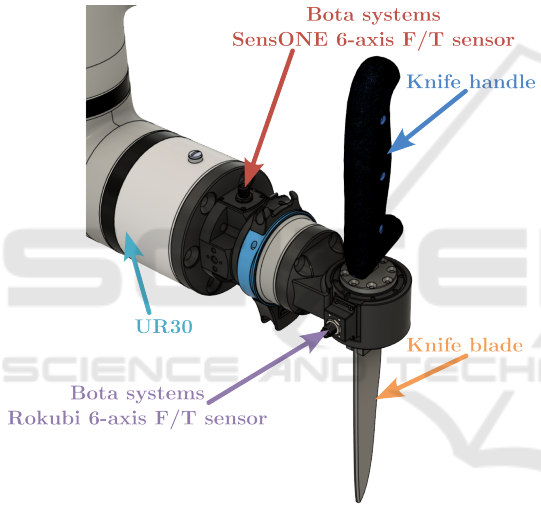

Figure 9: Knife prototype with PA-CF version of the single-sensor adapter.

(a) Top view (b) Bottom view

Figure 10: PA-CF single-sensor adapter views.

The component is made in one block and follows the same mechanical principles as the metallic version. However, as it is not recommend to create threaded holes in PA-CF, hexagonal recesses are incorporated to insert nuts, allowing the blade to be securely fastened to the assembly.

3.1.3 Dual-Sensor Configuration for Force Decoupling

This configuration integrates two Rokubi sensors to simultaneously measure both cutting and operator-applied forces. By directly capturing these two force sources, the design improves measurement accuracy and reduces the need for complex estimation or post-processing.

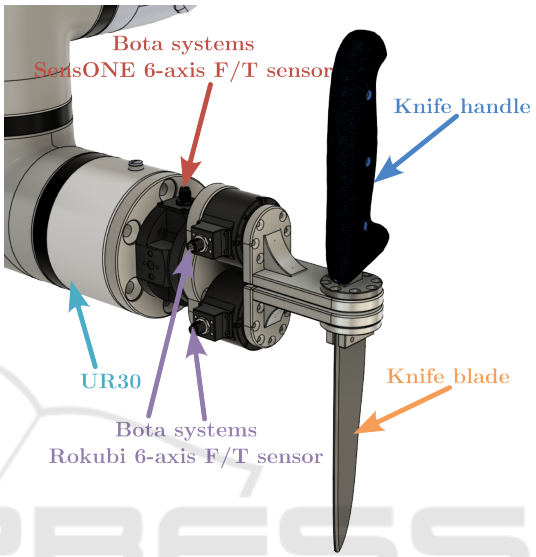

Figure 11: Knife prototype with two additional force/torque sensors.

The assembly consists of three machined aluminium components (Aluminium 5083): a central interface connecting the main and additional sensors, and two parts mounted on each Rokubi sensor. This arrangement decreases the distance between the handle and the blade compared to the single-sensor version, improving ergonomics.

Figure 12: Central interface part connecting the two Rokubi sensors with the main sensor.

The components connecting the Rokubi sensors to the handle and the blade, as shown in Figure 13, consist of three parts: the first mounts onto the Rokubi sensor, the second attaches the measured component (either the blade or the handle), and the third positions and reinforces the overall assembly.

As previously described, threaded holes and cylindrical dowel pin holes are incorporated to ensure pre-

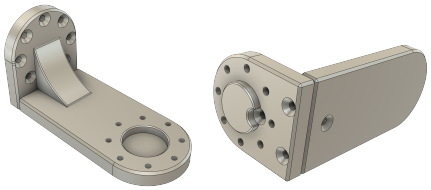

(a) Top view (b) Bottom view

Figure 13: Mounting components attached to the Rokubi sensors.

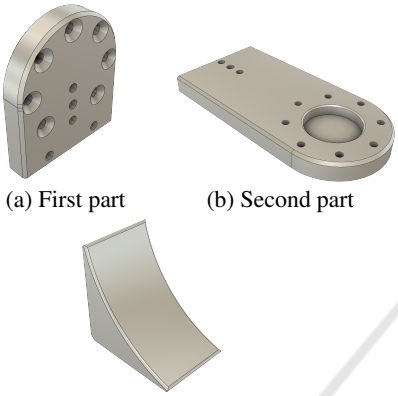

(a) First part (b) Second part

(c) Third part

Figure 14: Three-part mounting structure.

cise alignment and secure assembly of all parts, including the force sensors.

The second element, shown in Figure 14b, was designed with a length of 84 mm to prevent any contact between the user's hand holding the handle and the rest of the adapter. This clearance ensures ergonomic handling while avoiding interference with the structural or sensor components during operation. To verify the structural integrity of this component, a simplified beam deflection analysis was conducted. The aluminium section is modelled as a cantilever beam of length L, fixed at $x = 0$ and subjected to a vertical force $F_{\text{ext}} = 200\,\text{N}$ at the free end ($x = L$), as illustrated in Figure 15.

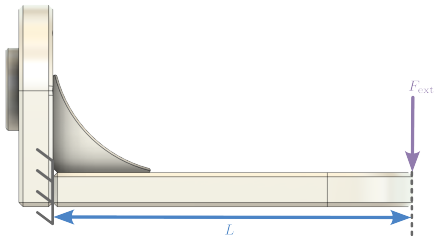

Figure 15: Model used for structural deflection analysis of the second adapter element.

The beam has a rectangular cross-section with width $b = 40 \times 10^{-3}\,\text{m}$, height $h = 8 \times 10^{-3}\,\text{m}$, and is made of Aluminium 5083 with a Young's modulus of $E = 71 \times 10^{9}\,\text{Pa}$. The second moment of area is calculated as $I = \frac{b\,h^3}{12}$.

According to strength of materials theory, the vertical deflection at any point $x \in [0, L]$ under this loading condition is given by:

$$v(x) = \frac{F\,x^3}{6\,E\,I}$$

Applied at the free end ($x = L = 0.084\,\text{m}$), the expression becomes:

$$v(L) = \frac{F\,L^3}{6\,E\,I} \approx 0.163\,\text{mm}$$

This simulation confirms that under a representative cutting force of 200 N, the expected elastic deformation remains below 0.2 mm, ensuring that no collision occurs between the upper and lower structural elements of the tool (see Figure 11), given the 2 mm clearance designed between the two components. This mechanical stability prevents unintended contact that could compromise measurement accuracy, while also minimising the distance between the handle and the knife blade, which is essential for maintaining an ergonomic tool geometry.

3.1.4 Knife Handle Prototypes

The knife handle was modelled from a 3D scan of a real industrial knife, commonly used in meat processing. This scan served as a realistic basis for designing functional handle prototypes, which were manufactured using PLA filament through FDM (Fused Deposition Modeling) 3D printing.

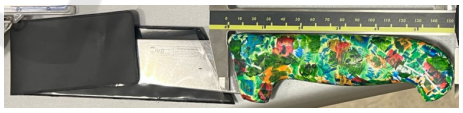

Figure 16: Industrial knife used as design reference.

Figure 17: PLA knife handle.

To ensure mechanical robustness, the PLA handle is mounted onto a substructure made of welded 2085 steel, which serves as the internal support and

structural backbone. This rigid interface ensures stable and repeatable performance during high-force cutting tasks.

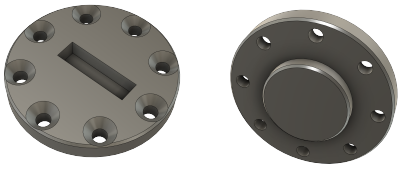

(a) Top side (b) Bottom side

Figure 18: First structural part supporting the handle.

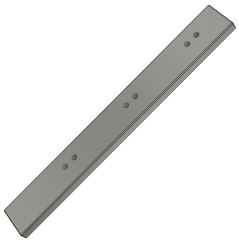

Figure 19: Second part of the handle attachment.

Both steel parts are welded together to form a rigid connector, as shown in Figure 20a. The final assembled handle, integrating both the PLA outer shell and the internal steel support, is presented in Figure 20b.

(a) Welded connector (b) Assembled handle

Figure 20: Knife handle prototype.

Sensitive Knife Handle

As previously mentioned, to predict the butcher's intentions and enable smooth re-orientation of the end-effector without perceived friction, a sensitive knife handle was prototyped. In the current setup (Figure 21), the handle is equipped with six off-the-shelf tactile pressure sensors (Interlink FSR®).

3.2 Sensorized Plier for Doll Demoulding

The primary objective of the design was to develop a sensorized tool capable of capturing, during human execution of the demoulding task, the three essential variables required for robotic imitation: pulling force,

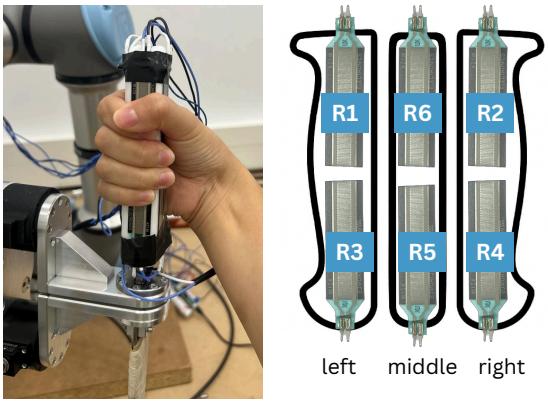

Figure 21: Force Resistive Sensor placement on the handle.

3D orientation, and spatial trajectory. This data acquisition had to be performed without interfering with the operator's natural movements and while meeting ergonomic and mechanical robustness requirements for a functional tool.

The development started from an experimental tool used in the SoftManBot project, which was based on a commercial pair of pliers fitted with an NGIMU sensor encapsulated in a 3D-printed housing attached to the end of one handle. This initial prototype enabled the recording of orientation and acceleration but lacked force sensing and full access to raw sensor data, limiting its usefulness for tasks requiring a complete characterization of the physical interaction during demoulding.

Figure 22: Starting point for tool design.

To overcome these limitations, a complete redesign of the tool was undertaken using an iterative approach. Various configurations of inertial sensors were evaluated, including both commercial mod-

ules and custom-built solutions. Ultimately, a high-precision IMU composed of the ISM330DHCX sensor and the MMC5983MA magnetometer was selected. This choice was based on its high sampling rate, excellent resolution, and low noise, enabling a more accurate reconstruction of orientation during the demoulding process. Unlike the previously used NGIMU module, this solution provides direct access to raw data, significantly reduces costs due to in-house assembly, and offers greater flexibility for implementing custom sensor fusion algorithms.

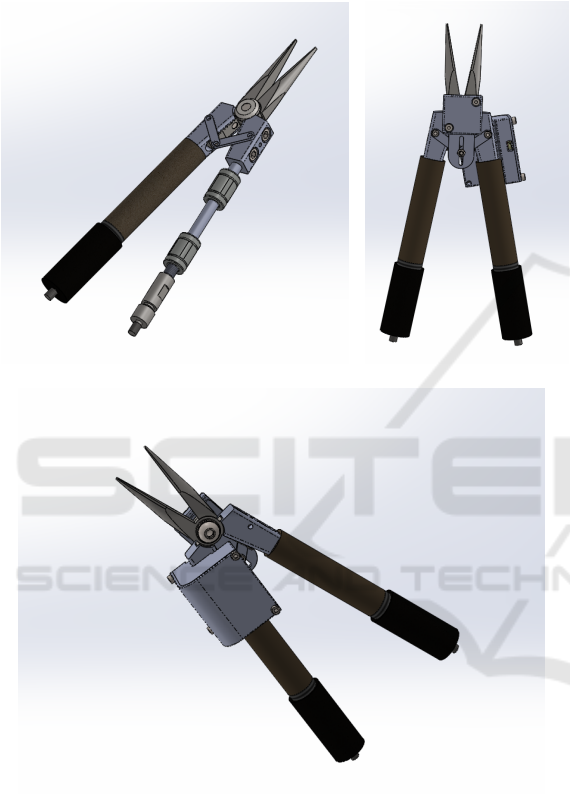

Figure 23: Current version of the tool at different stages of assembly.

The redesign began with a CAD model, which was subjected to finite element analysis (FEA) in SolidWorks to validate its structural resistance under typical demoulding loads. An initial prototype was 3D-printed to evaluate ergonomic aspects, sensor integration, and assembly feasibility. Following initial functional testing, the final prototype was constructed using specific materials for each component function: the head and jaws of the pliers were made from DIN 1.0401 (C15) steel, while the metallic handle frame was fabricated from DIN 1.0503 (C45) steel. The handle covers and housings for the force sensors were 3D-printed in PA12 polyamide, as were the casings that house the IMU module, ESP32, ADC, and battery. Additionally, a custom part made of S275JR steel was designed to keep the IMU centered at the joint of the pliers, ensuring that the sensor remained aligned with the bisector of the angle formed by the handles during opening and closing.

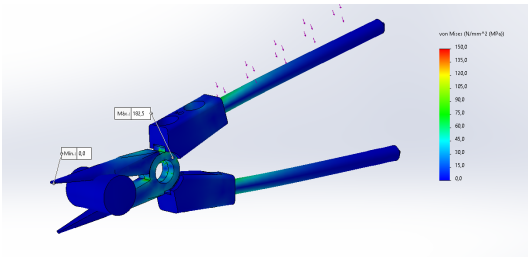

Figure 24: Finite Element Analysis of the pliers.

This material distribution ensures mechanical robustness in load-bearing areas, lightweight construction in electronic integration zones, and geometric stability for the sensor's orientation, all while maintaining an ergonomic and functional design suitable for operator use.

3.2.1 Sensing and Integration Architecture

The final design of the tool integrates the following components:

- **Force Sensing:** Two inline load cells (model DYMH-106, 0–20kg), one in each handle, measure the pulling force applied by the operator. The differential signals from both cells are electrically combined to form a full Wheatstone bridge, which is connected to a NAU7802 analog-to-digital converter (ADC). This configuration provides a measurement of the net pulling force exerted between the two handles.
- **Inertial Sensing:** A 9-DoF IMU module (ISM330DHCX + MMC5983MA) installed at the pivot axis of the pliers records linear acceleration, angular velocity, and the Earth's magnetic field. These data are fused using a Madgwick filter to reconstruct the full orientation of the system in real time as Euler angles. The inclusion of the magnetometer is particularly important for correcting yaw drift, enabling a stable heading estimate that is critical for robotic imitation of human strategies.
- **Acquisition and Communication Unit:** An ESP32-S3 Zero manages data acquisition via I2C, synchronizes all signals, and transmits the data in real time to a ROS node over Wi-Fi. All electronics, including the LiPo battery and boost converter used to power the load cells, are integrated into one of the handles.

3.2.2 Sensor Calibration

IMU Calibration

In the final prototype, the NGIMU sensor was replaced with a more precise solution based on the ISM330DHCX + MMC5983MA pair. This new configuration improves both the resolution and the sampling frequency of the inertial sensors. The ISM330DHCX maintains the 16-bit resolution of the accelerometer and gyroscope but increases the sampling rate from 400Hz (in the NGIMU) to 833Hz, allowing for more accurate capture of fast and transient movements.

As for the magnetometer, the one used in NGIMU offered a wider range (±1300µT), but with a resolution of only 0.3µT/LSB, an RMS noise of approximately 0.5–1µT, and a maximum acquisition rate of 20–75Hz. In contrast, the MMC5983MA provides a range of ±800µT but achieves a resolution of up to 0.00625µT/LSB in 18-bit mode, total noise as low as 0.04µT RMS, and an acquisition frequency of up to 100Hz. These improvements enable a much more accurate and stable estimation of the magnetic field, which is particularly beneficial for correcting yaw drift during sensor fusion. As a result, heading precision is significantly improved, reducing the orientation error from ±1 degree with the NGIMU to ±0.5 degrees with the new system.

In addition to improved performance, this new setup provides better control over the acquired data, the ability to automatically compensate thermal drifts, reduced power consumption, and a significantly lower unit cost, making it more suitable for embedded integration and scalable applications.

The gyroscope and accelerometer were manually calibrated using a custom-made acrylic cube designed to place the IMU in the six principal orientations (±X, ±Y, ±Z). This approach allowed for determining the static bias of each axis under well-defined resting conditions. Regarding the magnetometer, its calibration was particularly critical to achieve accurate yaw estimation, which is key to full orientation reconstruction during demoulding. For this purpose, a yaw/pitch/roll calibration jig was built using acrylic and nylon screws to avoid magnetic interference. Inspired by the procedure described in (Heeb, 2008), this device enabled controlled rotation along all three axes, keeping the IMU at the center of the structure, while the ESP32, charging system, and battery were distributed around the jig in a layout similar to their final arrangement in the tool, in order to replicate realistic magnetic conditions during calibration.

During the calibration process, two types of magnetic distortions were identified and compensated:

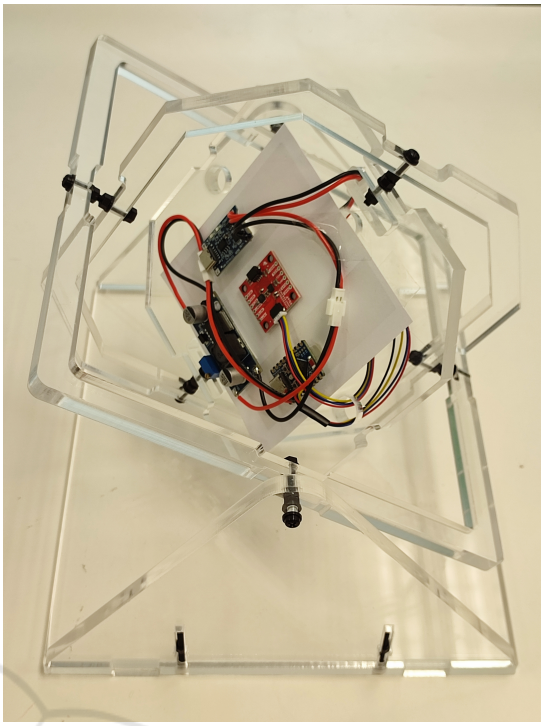

Figure 25: Yaw/pitch/roll jig built for magnetic calibration.

- **Hard Iron Distortion:** caused by static magnetic fields generated by nearby ferromagnetic materials or permanent magnets, which shift the center of the expected measurement sphere.
- **Soft Iron Distortion:** directional distortions caused by conductive or magnetic materials near the sensor, which deform the sphere into an ellipsoid due to interaction with the Earth's magnetic field.

To correct these distortions, a geometric calibration was performed by fitting an ellipsoid to the 3D data cloud obtained during a complete manual sweep. This fitting allowed for the estimation of:

1. The ellipsoid center $b = [x_c,\ y_c,\ z_c]^T$, associated with the hard iron effect.
2. The inverse transformation matrix A^{-1}, which corrects scaling factors and axis misalignments (soft iron effect).

The general equation used to compute the calibrated reading h_c from the measured magnetometer data h_m is:

$$h_c = A^{-1} \cdot (h_m - b) \tag{1}$$

Where:

- $h_m \in \mathbb{R}^3$ is the raw magnetometer reading,
- b is the bias vector (offset),

- A^{-1} is the inverse matrix that transforms the ellipsoid into a unit sphere. This matrix includes scaling factors and possible minor rotations due to non-orthogonal axis distortions.

The estimation of $\mathbf{A}$ and $\mathbf{b}$ is performed using a least-squares ellipsoid-specific fitting approach, which minimizes the algebraic distance of the measured points to a general quadric surface under geometric constraints. This method corresponds to case $k = 4$ in the paper *Least Squares Ellipsoid Specific Fitting* by Li and Griffiths [3] (Li and Griffiths, 2004).

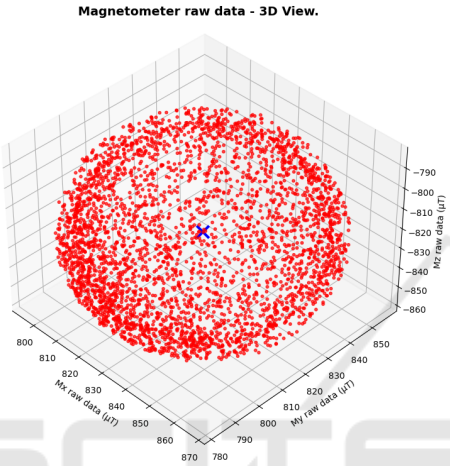

Figure 26: Magnetometer raw data (3D view).

Figure 26 shows the 3D representation of the point cloud obtained during calibration. Figure 27 shows the orthogonal projection on the XY, XZ, and YZ planes, respectively.

After applying this calibration, an improvement was observed in the uniformity of the magnetic field magnitude, which is a strong indicator of effective distortion compensation. The calibration process was validated through 3D visualization and statistical metrics on the sphericity of the calibrated point cloud.

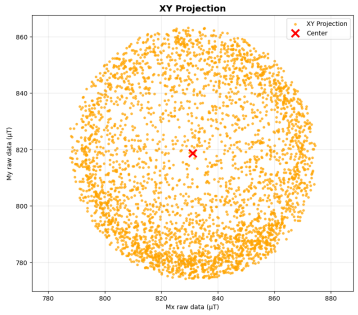

(a) XY projection

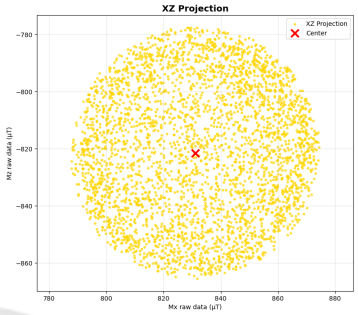

(b) XZ projection

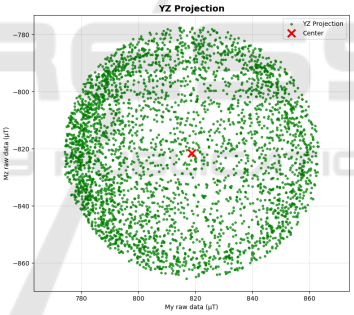

(c) YZ projection

Figure 27: Projection of the point cloud on the main orthogonal planes.

Load Cell Calibration

To characterize the load cells, a UR16e robot was used in force control mode to apply controlled traction along the Z-axis on the sensorized tool, with forces ranging from 0 to 200N. The forces were applied incrementally, and raw acquisition data were captured for subsequent filtering and calibration.

The sensing system consists of two inline load cells (model DYMH-106), each with a 20kg capacity, a sensitivity of $0.8 \pm 20\%$ mV/V, and an accuracy of 0.5% full scale (linearity + hysteresis + repeatability). These cells provide differential output and feature IP67-rated enclosures. They are mounted inside the tool handles and connected electrically to form a single Wheatstone bridge, which outputs a combined force signal. Although the manufacturer recommends an excitation voltage between 5 and 15V, in this application all components are powered at 3.3V directly from the ESP32-S3 Zero. Before considering the use of a voltage booster and external ADC reference, the system was tested at 3.3V with moderate gain, confirming linear behavior across the entire operational range. Under these conditions, the expected maximum output from the differential SIG+/SIG– lines is approximately 2.64mV, which falls within the sensitivity range accepted by the NAU7802.

The Wheatstone bridge signal is acquired using

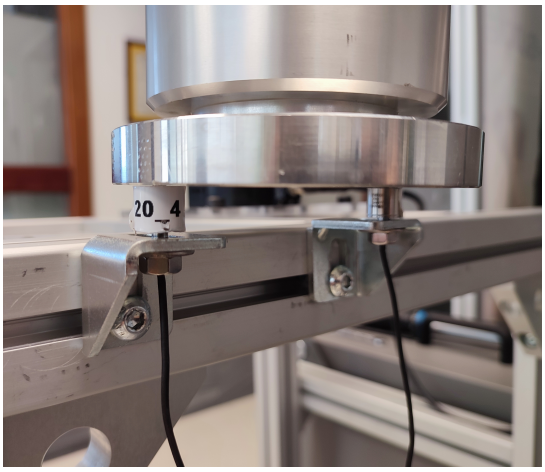

Figure 28: Calibration of load cells with the UR16e robot.

the NAU7802, a 24-bit ADC with an integrated amplifier specifically designed for load cell applications. This device includes digital filtering to effectively suppress 50Hz and 60Hz interference, which is common in industrial environments with power line noise. To further reduce high-frequency noise, a sliding window averaging filter was implemented in firmware. The window length is configurable, allowing for noise attenuation without introducing significant measurement delay.

During calibration, the raw data were fitted to a linear curve using least squares, yielding the corresponding scale factor (slope) and offset coefficients for converting raw readings into force values expressed in Newtons:

$$Force(N) = m \cdot Raw\_measure + b \quad (2)$$

The analysis confirmed a strictly linear response across the full operational range, with an average error of 0.64%, validating the suitability of both the sensor and the signal conditioning system.

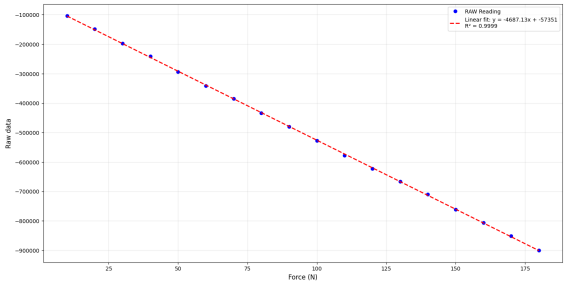

Figure 29: Load cells characterization representation.

Although the manufacturer specifies a thermal drift of ±0.05% F.S./10°C in both offset and sensitivity, this effect is considered negligible under normal working conditions. Nevertheless, the NAU7802 includes an internal temperature sensor, whose readings are used in the firmware to apply automatic temperature compensation, thereby minimizing potential errors caused by thermal variations during use.

3.2.3 Data Synchronization and Publishing

All sensors are connected to a single I2C bus in series configuration, managed by the ESP32-S3. Data acquisition is performed at a constant frequency (up to 100Hz), and readings are timestamped locally for synchronization. The microcontroller transmits the structured data packets via Wi-Fi to a ROS node on an external PC. There, the data streams (force, IMU, and visual position) are integrated into a unified timestamped structure for further analysis, visualization, or use in learning algorithms.

4 EXPERIMENTAL VALIDATION

4.1 Evaluation of Cutting Forces for the Knife End-effector

To evaluate the general force transmission during a meat-cutting operation, a mock-up test was conducted using a rigid fixture placed on top of a force sensor to better observe the forces involved. The testing setup included the end-effector prototype (Figure 11) equipped with two additional force sensors (Botasys Rokubi), as shown in Figure 30. The knife end-effector was mounted on a UR5e robotic arm, which was controlled in Freedrive mode. A human operator applied force along the y-axis in a back-and-forth motion, as indicated in the same figure. A comparison between the applied force (at the handle side) and the perceived force yielded a root mean square error (RMSE) of 2.88 N.

To record the hand grip during the experiments, six resistive tactile sensors were placed on the knife handle. The readings from these sensors were transformed into a color-coded tactile image for each time instant, as demonstrated in Figure 32.

4.2 Evaluation of Demoulding Forces for the Sensorized Plier

4.2.1 Orientation Validation via Comparison with UR16e

To validate the accuracy of the inertial system, the tool was mounted on the tool of a UR16e collaborative robot and subjected to known translational and rotational movements. The orientation readings (Euler angles) provided by the IMU were compared with

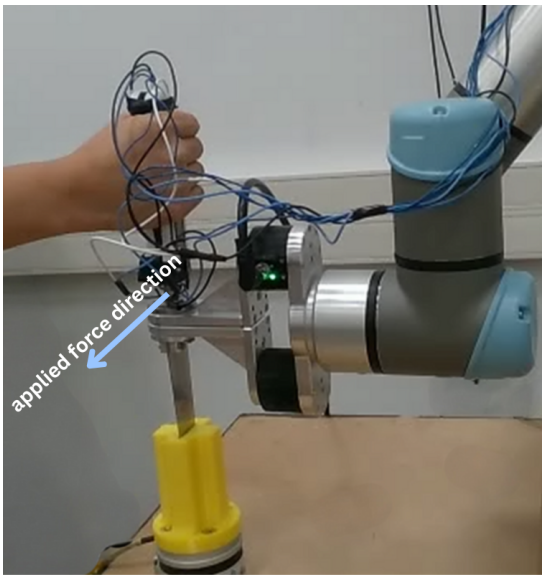

Figure 30: Force testing with the knife end-effector with two additional force/torque sensors. The yellow plastic fixture below is fixed on an OnRobot HEX-E force/torque sensor which is taken as a measure of the ground truth of the force applied by the knife blade.

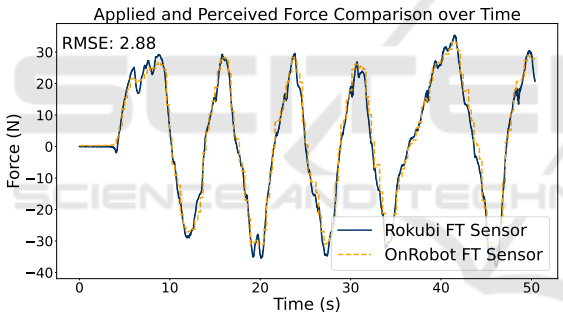

Figure 31: Comparison of force measurements between the Rokubi sensor integrated into the knife end-effector and the HEX-E sensor positioned to receive force from the knife blade. The RMSE between the two signals is 2.88 N, indicating a close alignment between applied and perceived forces.

the kinematic estimates generated by the UR Server within the ROS environment.

The comparisons showed a close match between both systems, with minor errors in the pitch and roll axes and good yaw stability due to drift compensation using the magnetometer. This validation confirms that the system can provide reliable real-time orientation estimates, even under transient accelerations.

4.2.2 Force Testing with Simulated Mold and Bota Systems Sensor

To evaluate the dynamic response of the force sensors during a realistic demoulding operation, a mockup

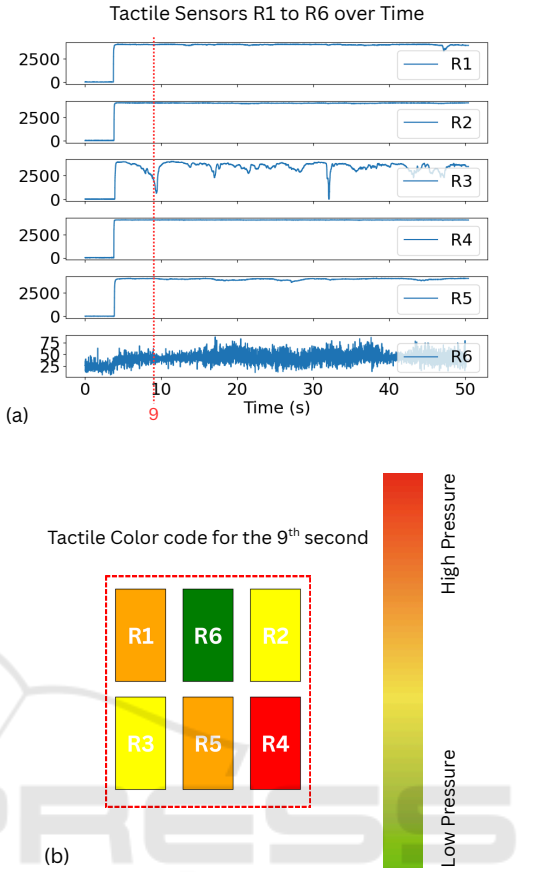

Figure 32: Six resistive tactile pressure sensors are attached to the knife handle. In (a), the plots show the pressure values recorded during the experiments described in Figure 30. To visualize the grip types and applied pressure, the sensor readings were color-coded at each time instant, as shown in (b). Preliminary tests are currently being conducted to predict the human operator's intention by feeding these tactile pressure images into neural networks.

was built using a doll part inserted into a simulated mold. This setup was placed on a 6-axis force-torque sensor from Bota Systems, capable of accurately measuring forces (F_x, F_y, F_z) and torques (M_x, M_y, M_z) at high frequency.

Manual extractions were performed using the sensorized pliers while simultaneously recording:

- The forces applied to the tool via the integrated load cells.
- The reaction forces within the part–mold system, measured by the Bota sensor.

This dual measurement setup allowed for a quantitative validation that the tool's load cells correctly reflect the actual force exerted—both in magnitude and direction. Clear correlations were observed between the peaks of pulling force and the normal forces ex-

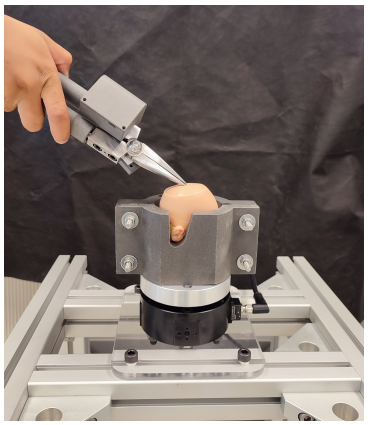

Figure 33: Force testing with the Bota Systems sensor.

erted on the mold during the critical moments of demoulding.

The comparative analysis showed an average difference of 3.28% between both measurements. However, this value must be interpreted in light of the cumulative measurement errors from both the Bota sensor and the tool's load cells, as well as the error introduced when calculating the net force by projecting it along the extraction axis using the orientation angles provided by the IMU.

5 DISCUSSION

A common thread across both case studies is the use of embedded sensorized tools to capture human manipulation strategies in tasks involving deformable objects. While the knife and the pliers address different industrial contexts—meat processing and doll manufacturing, respectively—both tools were designed to overcome the limitations of external sensing systems by integrating multimodal perception directly into ergonomic hand tools. This approach enables the faithful recording of forces, orientations, and trajectories without interfering with natural operator behaviour, thereby facilitating knowledge transfer to collaborative robots.

The quantitative results obtained provide insight into the practical suitability of these tools for Learning from Demonstration (LfD). In the knife case, the observed root mean square error (RMSE) of 2.88 N between the integrated sensor and the reference system indicates a high level of fidelity in force estimation. Considering that typical cutting forces often exceed 100 N, this error margin is relatively small, suggesting that the captured data are sufficiently accurate for training robotic systems to reproduce cutting strategies.

For the pliers, the average difference of 3.28% compared to the Bota Systems force–torque sensor confirms the ability of the embedded load cells to reflect real extraction forces during demoulding. Although this discrepancy arises in part from accumulated measurement uncertainties and the projection of forces along the extraction axis, the error remains within an acceptable range. Importantly, LfD frameworks do not require exact replication of absolute force values; instead, they benefit from consistent and accurate capture of relative patterns of pulling and twisting that characterize the human strategy.

A potential concern when integrating multiple sensors into a single tool is the possibility of mutual interference, particularly when forces are applied simultaneously during manipulation. In the case of the pliers, the two inline load cells are mechanically isolated within the handles and electrically combined into a full Wheatstone bridge, which provides a net force measurement while inherently canceling crosstalk. Experimental calibration against a reference force–torque sensor confirmed linearity and negligible interference between the two sensors. For knife prototypes, multiple force-torque sensors were used in parallel, but each was rigidly mounted in a mechanically decoupled configuration to separately capture the operator-applied and task-induced forces. Although some redundancy exists by design, mechanical adapters and careful alignment minimized the risk of cross-influence.

Taken together, these results highlight the practical implications of sensorized tools for skill transfer. The measured errors both in absolute force (knife) and in relative accuracy (pliers) are sufficiently low to enable successful robotic imitation of complex manual tasks. More critically, they demonstrate that task-specific tool design can balance ergonomic usability with high-quality data acquisition, which is essential for bridging the gap between human expertise and robotic execution.

Nevertheless, certain limitations must be acknowledged. Both case studies were conducted in controlled scenarios and further testing is necessary in industrial environments to assess robustness under variability in materials, operator behavior, and long-term use. Future work should also explore the extent to which sensing inaccuracies affect actual task success when demonstrations are transferred to robots. In addition, extending the toolset with complementary sensing modalities like tactile arrays for the pliers or additional multi-axis force sensing for the knife may further improve robustness and generalization across tasks.

6 CONCLUSIONS

This work contributes to the automation of deformable object manipulation by introducing sensorized handheld tools designed to capture human strategies during soft object handling. Focusing on two representative tasks, such as demoulding of vinyl parts in toy manufacturing and meat cutting in food processing, the study presents the design and validation of custom end-effectors equipped with multimodal sensing capabilities. The plier tool integrates inline load cells and an inertial measurement unit (IMU) to record force and orientation data under realistic working conditions using a simulated mold. The knife tool setup includes multiple force/torque sensors and a sensorized handle, tested in a Freedrive mode against a static fixture. All components were synchronized via ROS, enabling consistent data acquisition for future Learning from Demonstration (LfD) applications. While full cobotic manipulation and LfD reproduction are beyond the scope of this study, the experimental results confirm the tools' ability to capture nuanced manipulation strategies without interfering with natural operator behavior. These findings validate the feasibility of embedding multimodal sensing into handheld and robotic tools, laying the groundwork for future integration into collaborative robotic workflows. Future work will focus on closing the LfD loop by transferring captured demonstrations to robotic platforms and evaluating performance in real collaborative tasks. Additionally, the sensorized knife will be embedded into a multimodal feedback system to support real-time trajectory adaptation within robot control loops.

ACKNOWLEDGEMENTS

This work was funded by the Spanish Ministry of Science, Innovation and Universities (Ref. MICIU/AEI/10.13039/501100011033) through the research project FedeMINDex (Ref. CNS2024-154907), by the Interreg VI-B SUDOE Programme through the research project ROBOTA-SUDOE (Ref. S1/1.1/P0125), and by the European Union (European Regional Development Fund - ERDF). The authors would also like to thank Titouan Briançon and Matteo Proverbio for their valuable assistance during the experimental phase of this research.

REFERENCES

Aly, B. A., Low, T., Long, D., Baillie, C., and Brett, P. (2023). Robotics and sensing technologies in red meat processing: A review. *Trends in Food Science & Technology*, 137:142–155.

Choi, S., Zhang, G., Fuhlbrigge, T., Watson, T., and Tallian, R. (2013). Applications and requirements of industrial robots in meat processing. In *IEEE International Conference on Automation Science and Engineering (CASE)*.

de Medeiros Esper, I., From, P. J., and Mason, A. (2021). Robotisation and intelligent systems in abattoirs. *Trends in Food Science & Technology*, 108:214–222.

Heeb, B. (2008). A general calibration algorithm for 3-axis compass/clinometer devices. *CREG Journal*, pages 12–18.

Li, Q. and Griffiths, J. G. (2004). Least squares ellipsoid specific fitting. In *Proceedings of the Geometric Modeling and Processing Conference (GMP)*, pages 335–340. IEEE Computer Society.

Long, D., Khalil, W., and Martinet, P. (2014a). Force/vision control for robotic cutting of soft materials. In *IEEE/RSJ International Conference on Intelligent Robots and Systems (IROS)*.

Long, D., Khalil, W., and Martinet, P. (2014b). Robotic deformable object cutting: From simulation to experimental validation. In *European Workshop on Deformable Object Manipulation*.

Maithani, H., Ramon, C., Alexandre, J., Lequievre, L., Mezouar, Y., and Alric, M. (2021). Exoscarne: Assistive strategies for an industrial meat cutting system based on physical human–robot interaction. *Applied Sciences*, 11(9):3907.

Mason, A., Romanov, D., Cordova-Lopez, L. E., and Korostynska, O. (2022). Smart knife: Integrated intelligence for robotic meat cutting. *IEEE Sensors Journal*, 22(21):20475–20483.

Nabil, E., Belhassen-Chedli, and Grigore, G. (2015). Soft material modeling for robotic task formulation and control in the muscle separation process. *Robotics and Computer-Integrated Manufacturing*, 32:37–53.

Sánchez-Martínez, D., Jara, C. A., and Gomez-Donoso, F. (2023). A new automatic method for demoulding plastic parts using an intelligent robotic system. *The International Journal of Advanced Manufacturing Technology*, 129:3109–3121.

Song, P., Corrales Ramón, J. A., and Mezouar, Y. (2022). Dynamic evaluation of deformable object grasping. *IEEE Robotics and Automation Letters*, 7(2):4392–4399.

Zakaria, M. H. D., Aranda, M., Lequièvre, L., Lengagne, S., Corrales Ramón, J. A., and Mezouar, Y. (2022). Robotic control of the deformation of soft linear objects using deep reinforcement learning. In *2022 IEEE 18th International Conference on Automation Science and Engineering (CASE)*, pages 1516–1522. IEEE.